NEW POSSIBILITIES OF OBLIQUE IONOSPHERIC SOUNDING USING PHASED ANTENNA ARRAYS

©2025 I.A. Moiseev [1,*], Z.V. Suvorova [2], V.V. Nikishov [3], A.V. Nikishov [3], I.V. Mingalev [2], V.N. Shubin [4], A.M. Merzlyi [1], A.T. Yanakov [1]

[1] *Space Research Institute RAS (IKI RAS), Moscow, Russia*

[2] *Polar Geophysical Institute (PGI), Murmansk, Apatity, Russia*

[3] *Experimental Design Bureau "Elanor", Moscow, Russia*

[4] *Pushkov Institute of Terrestrial Magnetism, Ionosphere and Radio Wave Propagation RAS (IZMIRAN), Moscow, Troitsk, Russia*

**e-mail: moiseeviaiki@yandex.ru*

Received August 27, 2023

Revised October 28, 2024

Accepted December 12, 2024

Additional possibilities of the oblique ionospheric sounding method with elevation and azimuth measurements of shortwave radio signal ray trajectories using receiving and transmitting ring-type phased antenna arrays with software-controlled directional pattern are discussed. For a mid-latitude radio path, comparisons of experimental measurements of arrival angles of single-hop propagation modes at the receiving point with ray trajectory calculations for this radio path were conducted over four days, using the empirical ionospheric model GDMI developed at IZMIRAN. It is shown that during morning hours from 06:00 UT to 7:30 UT, there is good agreement between measured and calculated arrival angles, while during daytime, minor corrections to the GDMI model-calculated ionospheric plasma parameter distributions are required to achieve similar agreement.

DOI: 10.31857/S00167940250308e9

1. INTRODUCTION

The method of multi-frequency oblique ionospheric sounding (hereinafter OS) has been widely used over the past 50 years and consists of placing synchronized receiver and transmitter of linearly frequency-modulated radio signal in the high-frequency (hereinafter HF) range on the

Earth's surface at a sufficiently large distance from each other, with which the range of frequencies at which the signal passes along the radio path from the transmitter to the receiver is determined, and for each frequency in this range, the signal travel time is measured. The measurement results are usually presented in the form of ionograms of oblique radio sounding of the ionosphere - OSI. This method allows obtaining an altitude profile of electron concentration referenced to the midpoint of the radio path, assuming that the ray trajectories along which radio waves propagate deviate little from the plane containing the receiver, transmitter, and center of the Earth, and that these trajectories are almost symmetrical with respect to the midpoint [Brunelli and Namgaladze, 1988].

Both of these assumptions are violated in many cases for radio paths longer than 1000 km due to significant changes in electron concentration in horizontal directions in the area of the radio path. For example, on radio paths running in the meridional direction, at times when the terminator is near the radio path, the ray trajectories can significantly curve in horizontal directions, and the point of their reflection from the ionosphere can be displaced relative to the midpoint of the radio path by more than 200 km. In [Vertogradov et al., 2016], it is shown that on the Cyprus − Rostov-on-Don radio path, the azimuthal angle of arrival of the ray trajectory at the receiving antenna can deviate by 3−10° relative to the azimuthal angle of the direction from the receiver to the transmitter. For the stated reasons, it is not always possible to draw unambiguous conclusions about the spatial distributions of ionospheric plasma parameters from oblique sounding ionograms.

To ensure the effective operation of modern radio communication, radar, radio direction finding, and radio navigation systems, it is necessary to continuously monitor the ionosphere to adapt these systems to its current state. One approach is to use empirical models for calculating the spatial distributions of ionospheric plasma parameters, and to perform operational corrections of these models based on data from the ionosphere monitoring system. Correction of model parameters is an important applied task that allows for significantly improving the prediction of HF radio wave propagation, as well as improving empirical ionosphere models.

Due to the reasons outlined, it is important to further improve the accuracy of existing ionosphere diagnostic methods, including the OI (Oblique Incidence) method for estimating the spatial distribution of ionospheric plasma parameters in this region. Measuring elevation and azimuthal angles, with which ray trajectories enter the receiving antenna, allows determining

with some accuracy the boundaries of the area where ray trajectories are reflected from the ionosphere, and obtaining an estimate of electron concentration in this area. Thus, the capabilities of the OI method are significantly increased, particularly improving the reliability of operational correction of empirical models of ionospheric plasma parameter distribution. In studies [Vertogradov et al., 2010; 2013; 2016], an ionosonde-direction finder with linear frequency modulation was successfully used, and important results were obtained on HF radio wave propagation along multi-hop trajectories.

For the interpretation of OI ionosonde data, the following approach is usually applied [Kravtsov and Orlov, 1980; Budden, 1985; Krasheninnikov and Egorov, 2005; Andreev et al., 2007a; b; Krasheninnikov et al., 2017; 2018; Krasheninnikov and Shubin, 2020; Mingalev et al., 2021]. First, empirical or numerical models are used to calculate the distribution of ionospheric plasma parameters in the radio path area, and then calculations of HF radio wave propagation from transmitter to receiver are carried out using the geometric optics approximation. Based on these calculations, theoretical ionograms are constructed and compared with experimental ones. Based on the comparative analysis, conclusions are drawn about the accuracy of radio communication capability predictions using the selected empirical models.

In recent years, circular phased antenna arrays (hereinafter - PAA) with software-controlled directional patterns have been created for operation in the HF band, which allow measuring the angles of arrival of radio signals to the receiving PAA with good accuracy [Nikishov and Nikishov, 2019; Ludwig and Nikishov, 2021].

The first objective of this work is to demonstrate the possibilities of using the above-mentioned PAAs to verify the correspondence between the HF radio wave propagation conditions obtained in the experiment and those calculated using ray tracing and an empirical model of the ionosphere. The second objective of this work is to verify the above-mentioned correspondence of calculations conducted using the Global Dynamic Model of Ionosphere (GDMI) empirical model developed at IZMIRAN for four days. In this model, the main parameters of the *F* 2-layer of the ionosphere for quiet geomagnetic conditions are calculated according to the models described in [Shubin et al., 2013; Shubin, 2015; Shubin, 2017], which are built on the basis of ground-based ionospheric sounding data and electron density profiles obtained by radio occultation method using satellites. It should be noted that the GDMI model does not include the sporadic *E* -layer.

2. DESCRIPTION OF THE PHASED ANTENNA ARRAY USED IN THE EXPERIMENT

Currently, phased antenna arrays in the form of a ring of supporting masts have been developed and are being used, on which either transmitting or receiving antenna elements are located. The receiving and transmitting antenna arrays are designed as ring equidistant antenna systems (Fig.1). In general, these antenna systems can be single-ring or represent two or more geometric rings. Phased antenna arrays for transmitting electromagnetic energy are made in a wide frequency range of HF radio waves and allow the formation of directional radiation of radio signals [Nikishov and Nikishov, 2019; Ludwig and Nikishov, 2021].

Fig. 1.

The receiving phased antenna array (PAA) performs multi-channel processing of analog signals followed by digital processing. In the experiment, the PAA is constructed from omnidirectional antenna elements in the form of two mutually perpendicular horizontal vibrators for receiving signals of linear and elliptical polarization. The received radio signals are processed in a broadband multi-channel synchronous receiving device. The flat radio wave front is received by the aperture of antenna elements on the Earth's surface with some time delay relative to the reference antenna element. Simultaneous digital sampling of the signal from the antenna elements captures the amplitude and phase of the received signals for subsequent processing in the algorithm of a single-stage direction-finding device.

The algorithm of the direction-finding device converts the streams of time samples of the analog signal into samples of the digital Fourier transform, and for each Fourier sample, the solution of the problem of determining the maximum likelihood function in azimuth and elevation coordinates is performed. At each angular position of the electronic radiation pattern of the receiving PAA in azimuth and elevation, a current estimate of the level of the signal reflected from the ionosphere is calculated at the frequencies of the test transmitter radiation or in the observation band.

The experiment used a 32-channel PAA with a geometric placement diameter of 200 m and angular spacing of antenna elements of 11.25°, which provides radio signal reception and angular resolution of 10 angular minutes in azimuth and elevation with an array gain of 15 dB. The radiation patterns of the antenna elements are omnidirectional with a vertical signal reception angle of up to 82°. The antenna elements are manufactured with technological tolerances to achieve their identity in the PAA design up to 3°. Methods for correcting receiving paths in the

direction-finding device algorithm using control signals are applied to correct operational phase characteristic deviations of the PAA analog path.

In addition to the spatial and amplitude evaluation of the received test radiation source signal in the direction-finding device in a system with a phased array antenna (PAA), an assessment of the signal-to-noise ratio of the digital data transmission radio link is performed. This assessment is carried out within the operating signal of the OFDM type in the frequency band of the working signal. A feature of this assessment is the use of information about the elevation angle and azimuth of the maximum level of the reflected signal from the direction-finding device to configure the algorithm for spatial tracking of the maximum received signal for radio signal reception by the radio modem.

The transmitting PAA of the experiment was capable of providing omnidirectional radiation of the test signal or directional radiation, synchronized with the receiving PAA in terms of the spatial position of the ionosphere zone illumination.

Directional transmission of HF signals is also carried out using omnidirectional antenna elements of the "broadband vertical" type, which includes radiating antenna elements, a dielectric mast with a base and mounting elements for radiators and the output of a broadband amplifier for HF-band radio signals operating in class A. Information data, synchronization signals, and control signals are fed into controlled transmitters, each of which synthesizes a carrier signal with the required frequency and specified initial phase, onto which the data to be transmitted is transferred. The formed working signals are amplified and radiated by antenna elements. The initial phases
of the signals radiated by each antenna element have different values, which ensures the orientation of the resulting radiation pattern of the transmitting PAA with the required angular spatial parameters. The experiment used an active transmitting PAA of 16 elements on a diameter of 200 m, with angular placement of vibrators at 22.5°, a PAA gain of 24 dB, and an antenna amplifier power of no more than 30 W.

Thus, the operation of a radio link with PAA allows for the evaluation of real parameters of signals reflected from the ionosphere and considers them for verifying the adequacy of radio wave propagation model forecasts and their correction.

3. COMPARISON OF RADIO PATH MEASUREMENT DATA WITH CALCULATIONS

For numerical modeling of HF radio wave propagation, the geometrical optics approximation is used, taking into account the anisotropy of the ionospheric plasma caused by the geomagnetic field [Kravtsov and Orlov, 1980]. Ray trajectories are found by numerical integration of the eikonal equations with the refractive index in the Appleton-Hartree form using an explicit 4th-order Runge-Kutta scheme with Hamiltonian correction at each trajectory step [Mingalev et al., 2021]. To specify the distribution of plasma frequency and electron collision frequency in the ionosphere, the empirical ionosphere model GDMI developed at IZMIRAN, mentioned in the introduction, was used.

When HF radio waves propagate along single-hop trajectories with reflection of these trajectories from the *E* -layer of the ionosphere, there can be either two trajectories for ordinary and extraordinary modes, or four trajectories, namely, lower and upper for ordinary and extraordinary modes. When these trajectories are reflected from the *F* 2-layer of the ionosphere, there can also be either two trajectories for ordinary and extraordinary modes, or four trajectories, lower and upper for each of the two modes.

For comparison with measurement results, the ordinary mode and lower trajectory were chosen, since the amplitude of the received signal for it is most often the highest due to less geometric divergence of trajectories compared to the upper trajectory and less absorption compared to the extraordinary mode.

The following were accepted as initial data when conducting measurements:

1) coordinates of the transmitting phased antenna array and receiving phased antenna array;
2) gain coefficients and radiation patterns for receiving and transmitting phased antenna arrays;
3) day, local time or UT;
4) list (nominal values) of frequencies authorized for use in the transmitted signal.

For each selected frequency of the transmitted signal, the following measurements were taken every 10 seconds:

a) signal delay time (time of signal propagation along the path);

b) azimuthal angle and elevation angle of signal arrival at the receiving phased antenna array;

c) radio noise level at the location of the receiving phased antenna array;

d) signal-to-noise ratio during transmission of the measurement information package.

A comparison was made between the measured arrival angles of the ray trajectories of signals with the highest amplitude on the mid-latitude radio path Yeisk-Ostafyevo and the calculated ray trajectories for the ordinary wave for time periods from 06:00 UT to 12:00 UT for four dates: 21.06.2019, 23.09.2019, 20.12.2019, 22.06.2020. The measurements were taken every 10 seconds. Time averaging was not used. The results of comparing these measurements with calculation results were the same as for measurements at time points 15 minutes apart. For this reason, to reduce the length of the article, the comparison of instantaneous measurement results with calculation results is not presented for all measurements, but only for measurements at time points 15 minutes apart.

The transmitter coordinates are 38.240405° E, 46.691059° N, the receiver coordinates are 37.513582° E, 55.515567° N. For measurements, authorized signal frequencies were used, the values of which were lower than the experimentally obtained maximum usable frequency (MUF) at the time of measurement. At certain times, the experimentally obtained MUF exceeded the calculated MUF.

During the day of 21.06.2019 there was low magnetic and solar activity. The three-hour *ap* -index values were 5, 6, 4, 5, 5, 3, 5, 9, and the *F* 10.7 index was 66.5.

Table 1.

Table 1 presents the results of measuring the arrival angles of ray trajectories at the receiving phased array antenna for 21.06.2019 for those times when the frequency used in the experiment was less than the calculated MUF.

From the data in Table 1, it can be seen that at all the given time points, except for 6:30 UT, the measurement and calculation results correspond well to each other. For the 6:30 UT time point, the calculations resulted in two modes: 1 *F* 2 and 1 *E* for the ordinary wave at frequency 7.271 MHz. For the upper calculated mode 1 *F* 2, the elevation angle was about 23.5°, which agrees well with the measured elevation angle of 25°, and for the lower calculated mode 1 *E* , the elevation angle was about 9.5°. The calculated amplitude of the signal arriving at the receiver via the upper trajectory was significantly higher than the amplitude of the signal arriving via the lower trajectory. The experimental results show only the 1 *F* 2 mode. This can be explained by the fact that the amplitude method of measuring angles does not separate modes at the antenna aperture and works reliably only in single-mode operation. Thus, it can be considered that for the

moment under consideration, the calculation results using the GDMI model agree well with the measurements.

Fig. 2.

Figure 2 shows projections onto a vertical plane passing through the receiver and transmitter of the lower ray trajectory for the ordinary wave at frequency 7.271 MHz for the time point 6:15 UT and the ray trajectory for the ordinary wave at frequency 11.072 MHz for the time point 8:15 UT. Both projections of ray trajectories are presented in "range-height" coordinates. From Fig. 2, it can be seen that the reflection area from the ionospheric layer of the first trajectory is located at a height of 172 km in the *F* 2-layer, and for the second trajectory, this reflection area is at a height of 101 km in the *E* -layer of the ionosphere. It is also evident that the first trajectory has an upper section where the trajectory passes at heights close to the height of its reflection point, with an area extending about 200 km. For the second trajectory, this upper section extends no more than 50 km.

Table 2.

Table 2 presents the results of measuring the arrival angles of ray trajectories into the receiving phased array for those time points on 06/21/2019, when the frequency used in the experiment was higher than the calculated MUF. The arrival angles for the calculated MUF are also presented.

From the first row of Table 2 it can be seen that for the time 6:45 UT, the calculated MUF for the ordinary wave was lower than the real MUF by at least 0.5 MHz. At the same time, the reflection area of the one-hop trajectory from the ionosphere was at the level of the *E* -layer, which can be judged by the measured elevation angle. It can be seen that for the calculated trajectory of the radio signal propagation at the MUF frequency, the arrival elevation angle to the receiving antenna is 4.6° less than the measured angle. To achieve agreement between the calculation results and measurements, the GDMI model can be supplemented with a sporadic *E* -layer by increasing the electron density values near the maximum height of the regular *E* -layer in the reflection area of the ray trajectory at 6:45 UT on 21.06.2019 so that the critical plasma frequency approaches 2 MHz.

At other times shown in Table 2, the situation is similar to the one described above for 6:45 UT. The calculated predicted MUF is lower than the frequency at which communication was established in the experiment, by a value within 0.1−0.9 MHz. At the same time, the calculated

and experimentally measured arrival angles of ray trajectories to the receiving phased array differ by no more than 1.5°, which is a good correspondence. The elevation angles of the ray trajectories arriving at the receiving phased array do not exceed 13°, which means reflection of ray trajectories in the *E* -layer of the ionosphere.

During the day of 23.09.2019 there was low magnetic and solar activity. The values of the three-hour *ap* -index were 2, 0, 2, 3, 2, 5, 3, 3, and the *F* 10.7 index was 66.1.

Table 3.

Table 3 presents the results of measuring the arrival angles of ray trajectories to the receiving phased array for 23.09.2019 for those moments when the frequency used in the experiment was less than the calculated MUF for the ordinary wave. Table 4 presents the results of measuring the arrival angles of ray trajectories to the receiving phased array for those moments on 23.09.2019 when the frequency used in the experiment was greater than the calculated MUF. The arrival angles for the calculated MUF are also presented.

Table 4.

For the observation day of 09/23/2019, the following picture emerged. For time moments in the interval from 6:00 UT to 7:15 UT, the calculated MUF for the ordinary wave exceeded the signal frequency in the experiment. At these times, for ray trajectories for the ordinary wave calculated at the frequency used in the experiment, the elevation angles of arrival of ray trajectories at the receiving antenna matched those observed in the experiment with an accuracy of 2 to 5°. The reflection of ray trajectories occurred from the *F* 2-layer of the ionosphere. For time moments in the interval from 7:30 UT to 12:00 UT, the calculated MUF was lower than the frequency at which communication was carried out in the experiment, by a value within 0.4-1.6 MHz. In the experiment, the reflection of ray trajectories occurred from the *E* -layer of the ionosphere. To achieve agreement between calculation results and measurements, the GDMI model can be supplemented with a sporadic *E* -layer, increasing the electron density values in the region of the maximum height of the regular *E* -layer.

During the day of 12/20/2019 there was low magnetic and solar activity. The values of the three-hour *ap* -index were 9, 4, 4, 2, 6, 7, 4, 6, and the *F* 10.7 index was 70.

Table 5.

Table 5 presents the results of measuring the angles of arrival of ray trajectories at the receiving phased array for 12/20/2019 for those moments when the frequency used in the

experiment was less than the calculated MUF for the ordinary wave. Table 6 presents the results of measuring the angles of arrival of ray trajectories for the ordinary wave at the receiving phased array for those moments of 12/20/2019 when the frequency used in the experiment was greater than the calculated MUF. The angles of arrival for the calculated MUF are also presented.

From the data in Table 5, it can be seen that for December 20, 2019, during time periods from 6:00 UT to 8:00 UT, the calculated MUF for the ordinary wave exceeded the signal frequency used in the experiment. At these times, for the ray trajectories of the ordinary wave calculated at the frequency used in the experiment, the elevation angles of arrival at the receiving phased array were 4-7° less than the same angles observed in the experiment. The reflection of ray trajectories occurred from the *F* 2-layer of the ionosphere. To achieve agreement between calculation results and measurements, the GDMI ionosphere model can be corrected for these time periods by increasing the height of the *F* 2-layer maximum in the reflection area of the ray trajectory by 10-20 km.

Table 6.

From the data in Table 6, it can be seen that for December 20, 2019, during time periods from 8:15 UT to 11:00 UT, the calculated MUF for the ordinary wave was lower than the frequency at which radio wave propagation occurred in the experiment, by a value within the range of 1 to 2 MHz. In the experiment, the reflection of ray trajectories occurred from the *E* -layer of the ionosphere. The obtained results indicate that to achieve agreement between calculation results and measurements, the GDMI model for these time periods could be supplemented with a sporadic *E* -layer, slightly increasing the electron concentration values in the region of the regular *E* -layer maximum height in the area of ray trajectory reflection.

During the day of June 22, 2020 there was low magnetic and solar activity. The values of the three-hour *ap* -index were 3, 3, 2, 5, 5, 3, 3, 3, and the *F* 10.7 index was 67.6.

Table 7 presents the results of measuring the arrival angles of ray trajectories at the receiving phased array for June 22, 2020, for those time periods when the frequency used in the experiment was less than the calculated MUF for the ordinary wave.

Table 8 presents the results of measuring the arrival angles of ray trajectories at the receiving phased array for those time periods on June 22, 2020, when the frequency used in the experiment was greater than the calculated MUF for the ordinary wave. The arrival angles for the calculated MUF are also presented.

Table 7.

Table 8.

From the data in Table 7 shows that for the day 22.06.2020, during time periods from 6:00 UT to 8:15 UT and from 11:00 UT to 12:00 UT, the MUF calculated for the ordinary wave exceeded the signal frequency in the experiment. At 6:00 UT, the elevation angle of the ray trajectory arrival, calculated at the frequency used in the experiment, at the receiving phased array antenna was 21.3°, which was 6.7° less than the same angle observed in the experiment. This means that to achieve agreement between the calculation results and measurements, the GDMI ionosphere model can be corrected for this moment by increasing the height of the maximum *F* 2-layer in the reflection area of the ray trajectory from this layer by 10-20 km.

Also from Table 7, it can be seen that at 6:15 UT, the measured elevation angle of the ray trajectory arrival was 26°, while the calculations resulted in two ray trajectories with elevation angles of 21.4 and 14°. Calculations also showed that if at this moment the height of the maximum km, then the elevation angle of the calculated upper ray trajectory arrival will be 26.7°, which is close to the measured value of this angle. *F* 2-layer in the GDMI model is increased by 10

A similar situation occurs at 6:30 UT, when the measured elevation angle of the ray trajectory arrival was 27°, while this same angle for the calculated upper ray trajectory was 21.7°. When increasing the height of the maximum *F* 2-layer in the GDMI model by 10 km at this moment, the elevation angle of the calculated upper ray trajectory arrival will be 27.1°, which agrees well with the measured angle.

Also from Table 7, it can be seen that at 6:45 UT, the measured elevation angle of the ray trajectory arrival was 22°, while the calculations resulted in two ray trajectories with elevation angles of 21.9 and 13°. Thus, at this moment, the arrival angles of the calculated upper ray trajectory coincide with the measured arrival angles with good accuracy.

From the table 7 it is also visible that in the time intervals from 7:00 UT to 8:15 UT and from 11:00 UT to 12:00 UT, there is good agreement between the measurement results and calculations. The difference between the experimental and calculated arrival angles of the ray trajectories does not exceed 2°. In this case, the reflection of ray trajectories occurs from the *E* -layer, since the elevation angles of the ray trajectories do not exceed 13°. Thus, at these times, the GDMI model provides correct ionosphere parameters at the height of the *E* -layer maximum in

the area of ray trajectory reflection.

From the data in Table 8, it can be seen that for June 22, 2020, in the time intervals from 8:30 UT to 10:45 UT, the calculated MUF was 0.4−0.6 MHz lower than the signal frequency in the experiment, and the elevation angles of the ray trajectories did not exceed 13°. The latter means that the reflection of ray trajectories occurs from the *E* -layer. These facts indicate that to achieve agreement between calculation results and measurements, the GDMI model can be supplemented with a sporadic *E* -layer, increasing the electron concentration values in the vicinity of the regular *E* -layer maximum height in the area of ray trajectory reflection from the ionosphere.

Overall, out of 95 considered time moments, for 33 moments the calculated MUF exceeded the signal frequency in the experiments. Such cases were predominantly observed in the time interval from 06:00 UT to 08:00 UT. Among these cases, in 32 time moments out of 33, the ionosphere layer from which the ray trajectory reflected coincided for both calculated and experimental trajectories. The discrepancies in the values of measured and calculated elevation angles of the ray trajectory arrival at the receiving phased array antenna were no more than 4−7°, and in 65% of cases, the discrepancy ranged from 0.4 to 2.5°. For the azimuth of the radio signal ray arrival, the maximum discrepancy between the experiment and calculations was 5°, while in 65% of cases, the discrepancy ranged from 0.2 to 1.5°.

For the remaining 62 time points out of the 95 considered, the calculated MUF was lower than the signal frequency in the experiment, with discrepancies in the specified frequencies reaching 3.7 MHz. Predominantly, such cases were observed during the time intervals from 08:00 UT to 11:00 UT, i.e., around local noon. It is noteworthy that in all cases when the model-calculated MUF for the ordinary wave was less than the actual one, the experiment showed reflection of ray trajectories from the *E* -layer of the ionosphere. In all these cases, the GDMI model can be corrected by slightly increasing the electron concentration at the height of the *E* -layer maximum during daytime in the region of the ray trajectory reflection to ensure agreement between calculation and measurement results.

4. CONCLUSIONS

Comparison of the results of measuring the arrival angles of ray trajectories on the Yeysk-Ostafyevo radio path with the results of ray trajectory calculations performed using the empirical ionosphere model GDMI for 95 time points in the interval from 06:00 UT to 12:00 UT for the

dates of June 21, 2019, September 23, 2019, December 20, 2019, June 22, 2020, showed that in the morning hours from 06:00 UT to 7:30 UT and during daytime from 11:00 UT to 12:00 UT, there is generally good agreement between the measured and calculated arrival angles. At some time points from the listed intervals, there are discrepancies between the measured and calculated elevation angles, which can be eliminated if at these moments the height of the maximum of the *F* 2-layer of the GDMI ionosphere model is corrected. During daytime in the time intervals from 08:00 UT to 11:00 UT, there is some discrepancy between the measured and calculated elevation angles, which can be eliminated if at the specified times the GDMI model is supplemented with a sporadic *E* -layer by increasing the electron concentration values in the vicinity of the regular *E* -layer maximum height in the region of the ray trajectory reflection from the ionosphere.

The use of the ionosphere VS method with measurement of elevation angles, azimuth angles, and reflected signal level along beam trajectories entering the receiving phased antenna array allows to accurately determine the position of the reflection area of beam trajectories from the ionosphere and determine the electron concentration in this area, and thus, if necessary, allows operational correction of empirical models of ionospheric plasma parameter distribution.

For practical implementation of the ionosphere VS method with measurement of elevation angles, azimuth angles, and reflected signal level along beam trajectories, it is advisable to use ring-type phased antenna arrays with a diameter of 200 m or more, as such phased antenna arrays allow measuring the arrival angles of single-hop radio wave propagation modes with high accuracy when receiving a signal, and when transmitting, they allow the formation of high-frequency energy radiation in specified spatial directions. It is also important to develop more sophisticated methods for analyzing the wave field on the antenna array.

FUNDING

The work of Moiseev I.A., Merzlyi A.M., Yanakov A.T. was supported by the grant of the Ministry of Education and Science of Russia "COSMOS-D" No. FFWG-2022-0012.

REFERENCES

– *Andreev M.Yu., Blagoveshchensky D.V., Vystavnoy V.M., Mingalev V.S., Mingaleva G.I.* Interpretation of experimental data on short radio wave propagation on the Saint Petersburg –

Svalbard Archipelago route // Geomagnetism and Aeronomy. Vol. 47. No. 4. P. 534–542. 2007a.
– *Andreev M.Yu., Mingaleva G.I., Mingalev V.S.* Numerical modeling of the structure of the high-latitude ionospheric *F* layer and short radio wave propagation through it in the meridional direction // Geomagnetism and Aeronomy. Vol. 47. No. 4. P. 518–527. 2007b.
– *Bryunelli B.E., Namgaladze A.A.* Physics of the Ionosphere. Moscow: Nauka, 528 p. 1988.
– *Vertogradov G.G., Uryadov V.P., Vertogradova E.G., Ponyatov A.A.* Super-long-range sounding of the ionospheric channel using an ionosonde/direction finder with linear frequency modulation signal // Radiophysics and Quantum Electronics. Vol. 53. No. 3. P. 176–187. 2010.
- *Vertogradov G.G., Uryadov V.P., Vertogradov V.G., Vertogradova E.G., Kubatko S.V.* Ionosonde-radio direction finder with linear frequency modulation signal - a new tool for ionosphere research and radio wave propagation // Izv. vuzov. Radiophysics. Vol. 56. No. 5. P. 287-306. 2013.
- *Vertogradov G.G., Uryadov V.P., Sklyarevsky M.S., Valov V.A.* Oblique sounding of the ionosphere using an ionosonde-radio direction finder with linear frequency modulation signal // Izv. vuzov. Radiophysics. Vol. 59. No. 11. P. 991-1003. 2016.
- *Kravtsov Yu.A., Orlov Yu.I* . Geometrical optics of inhomogeneous media. M.: Nauka, 304 p. 1980.
- *Krasheninnikov I.V., Shubin V.N.* Frequency dependence of energy parameters of the wave field at the maximum range of one-hop radio wave propagation under conditions of low solar activity // Geomagnetism and Aeronomy. Vol. 60. No. 2. P. 220-228. 2020. https://doi.org/10.31857/S001679402002008X
- *Krasheninnikov I.V., Egorov I.B.* Formation of combined modes in ionospheric radio wave propagation // Geomagnetism and Aeronomy. Vol. 45. No. 2. P. 241-244. 2005.
- *Krasheninnikov I.V., Pavlova N.M., Sitnov Yu.S.* IRI model in the problem of predicting ionospheric radio wave propagation under conditions of high solar activity // Geomagnetism and Aeronomy. Vol. 57. No. 6. P. 774-782. 2017. https://doi.org/10.7868/S0016794017060050
- *Krasheninnikov I.V., Givishvili G.V., Stakhanova I.G.* Estimation of the critical frequency in the problem of radio sounding of the ionosphere from high-orbit spacecraft in the Arctic region //

Geomagnetism and Aeronomy. Vol. 58. No. 5. P. 669-675. 2018. https://doi.org/10.1134/S0016794018050097

- *Ludwig V.A., Nikishov V.V.* Passive location and countermeasures against precision-guided weapons systems. M.: LENAND, 256 p. 2021.

- *Mingalev I.V., Suvorova Z.V., Shubin V.N., Merzly A.M., Tikhonov V.V., Talalaev A.B., Mingalev V.S.* Differences in HF radio communication condition forecasts between a transmitter at mid-latitudes and a receiver in the Arctic region when using various empirical ionosphere models // Geomagnetism and Aeronomy. Vol. 61. No. 4. P. 506–519. 2021. https://doi.org/10.31857/S001679402104009X

– *Nikishov D.V., Nikishov V.V.* Decameter communication system through the ionosphere / Patent of the Russian Federation for invention No. 2680312 dated 20.02.2019.

– *Shubin V.N.* Global empirical model of the critical frequency of the *F* 2-layer of the ionosphere for quiet geomagnetic conditions // Geomagnetism and Aeronomy. Vol. 57. No. 4. P. 450–462. 2017. https://doi.org/10.7868/S0016794017040186

– *Budden K.G.* The propagation of radio waves. Cambridge: Cambridge University Press. 669 p. 1985.

– *Shubin V.N.* Global median model of the F2-layer peak height based on ionospheric radio-occultation and ground-based Digisonde observations // Adv. Space Res. V. 56. N 2. P. 916–928. 2015. https://doi.org/10.1016/j.asr.2015.05.029

– *Shubin V.N., Karpachev A.T., Tsybulya K.G.* Global model of the *F* 2 layer peak height for low solar activity based on GPS radio-occultation data // J. Atmos. Sol.-Terr. Phy. V. 104. P. 106 – 115. 2013. https://doi.org/10.1016/j.jastp.2013.08.024

Table 1. Values of measured and calculated arrival angles for 06/21/2019 for those moments when the calculated MUF for the ordinary wave exceeded the signal frequency in the experiment

Time UT	Signal frequency in the experiment, MHz	Measured azimuth, deg	Calculated azimuth, deg	Measured elevation angle, deg	Calculated elevation angle, deg
6:00	7.271	174	176.6	22	21.5
6:15	7.271	176	176.6	27	29
6:30	7.271	177	176.7	25	23.5 and 9.5
8:15	11.072	177	176.7	11	11.4
8:30	11.072	176	176.7	11	11.4
8:45	11.072	177	176.7	11	11.4
11:15	11.072	177	176.8	13	11.55

Table 2. Values of measured and calculated arrival angles of ray trajectories for those moments of the day on 06/21/2019 when the calculated MUF for the ordinary wave was less than the signal frequency in the experiment

Time UT	Signal frequency in the experiment, MHz	Calculated MUF, MHz	Measured azimuth, deg	Azimuth calculated for the calculated MUF, deg	Measured elevation angle, deg	Elevation angle calculated for the calculated MUF, deg
6:45	11.072	10.600	178	176.74	16	11.43
7:00	11.072	10.710	177	176.74	13	11.43
7:15	11.072	10.807	177	176.74	11	11.42
7:30	11.072	10.890	177	176.74	11	11.41
7:45	11.072	10.967	177	176.74	13	11.41
8:00	11.072	11.030	176	176.75	11	11.4
9:00	12.114	11.186	177	176.75	11	11.39
9:15	12.114	11.200	177	176.75	11	11.39
9:30	12.114	11.204	176	176.75	11	11.39
9:45	12.114	11.197	177	176.75	11	11.39
10:00	12.114	11.183	177	176.75	12	11.39
10:15	12.114	11.334	177	176.76	11	11.54
10:30	12.114	11.298	176	176.76	13	11.54
10:45	12.114	11.252	177	176.76	11	11.54
11:00	12.114	11.195	177	176.77	11	11.54
11:30	11.072	11.051	176	176.77	11	11.55
11:45	11.072	10.963	177	176.77	13	11.56

12:00	11.072	10.863	177	176.77	13	11.57

Table 3. Values of measured and calculated arrival angles for 09/23/2019 for those moments when the calculated MUF for the ordinary wave exceeded the signal frequency in the experiment

Time UT	Signal frequency in the experiment, MHz	Measured azimuth, deg	Calculated azimuth, deg	Measured elevation angle, deg	Calculated elevation angle, deg
6:00	7.325	173	176.1	26	22
6:15	7.325	175	176.2	25	23.4
6:30	7.325	171	176	28	23
6:45	7.325	175	176.7	29	23.3
7:00	7.325	177	176.8	25	23.7
7:15	7.325	179	177	26	24

Table 4. Values of measured and calculated arrival angles of ray trajectories for those moments of the day on 09/23/2019 when the calculated MUF for the ordinary wave was less than the signal frequency in the experiment

Time UT	Signal frequency in the experiment, MHz	Calculated MUF, MHz	Measured azimuth, deg	Azimuth calculated for the calculated MUF, deg	Measured elevation angle, deg	Elevation angle calculated for the calculated MUF, deg
7:30	11.072	9.880	175	176.7	13	11.5
7:45	11.072	10.160	177	176.7	18	12
8:00	11.072	10.210	175	176.7	13	11.8
8:15	11.072	10.280	178	176.7	12	11.8
8:30	11.072	10.327	178	176.7	13	11.8
8:45	11.072	10.364	177	176.7	13	11.8
9:00	11.072	10.388	173	176.7	13	11.6
9:15	12.114	10.398	175	176.8	11	11.6
9:30	12.114	10.395	177	176.8	11	11.6
9:45	12.114	10.378	178	176.8	11	11.6
10:00	12.114	10.347	175	176.8	13	11.6

10:15	11.072	10.303	177	176.8	13	11.6
10:30	11.072	10.245	177	176.8	13	11.6
10:45	11.072	10.172	173	176.8	13	11.6
11:00	11.072	10.085	178	176.8	13	11.7
11:15	11.072	9.9816	177	176.8	13	12
11:30	11.072	9.8630	173	176.8	13	12
11:45	11.072	9.7278	175	176.8	13	11.8
12:00	11.072	9.5748	178	176.8	13	11.8

Table 5. Values of measured and calculated arrival angles for 12/20/2019 for those moments when the calculated MUF for the ordinary wave exceeded the signal frequency in the experiment

Time UT	Signal frequency in the experiment, MHz	Measured azimuth, deg	Calculated azimuth, deg	Measured elevation angle, deg	Calculated elevation angle, deg
6:00	7.271	173	176.1	27	21.4
6:15	7.271	174	176.2	26	20.4
6:30	7.271	171	176.3	27	20
6:45	7.271	178	176	25	19.4
7:00	7.271	177	176.1	26	19.2
7:15	7.271	173	176.2	23	19.1
7:30	7.271	170	176.3	27	19
7:45	7.271	173	176.4	26	19
8:00	7.271	173	176.5	23	18.9

Table 6. Values of measured and calculated arrival angles of ray trajectories for those moments of the day on 12/20/2019 when the calculated MUF for the ordinary wave was less than the signal frequency in the experiment

Time UT	Signal frequency in the experiment, MHz	Calculated MUF, MHz	Measured azimuth, deg	Calculated azimuth, deg	Measured elevation angle, deg	Calculated elevation angle, deg
8:15	11.072	10.113	178	176.6	17	22.9
8:30	11.072	10.200	173	176.7	14	22,8
8:45	11.072	10.200	174	176.7	12	22,8
9:00	11.072	10.500	171	176.7	13	24

9:15	11.072	10.500	177	176.8	13	24
9:30	11.072	10.250	175	176.8	13	22,7
9:45	11.072	10.210	174	176.8	11	22,8
10:00	11.072	10.060	177	176.8	12	23
10:15	11.072	9.900	176	176.8	13	23
10:30	11.072	9.760	177	176.8	14	23,9
10:45	11.072	9.570	175	176.8	12	24
11:00	11072	9.190	177	176.8	13	23,2

Table 7. Values of measured and calculated arrival angles for 06/22/2020 for those moments when the calculated MUF for the ordinary wave exceeded the signal frequency in the experiment

Time UT	Signal frequency in the experiment, MHz	Measured azimuth, deg	Calculated azimuth, deg	Measured elevation angle, deg	Calculated elevation angle, deg
6:00	7.325	177	176.6	28	21.3
6:15	7.325	176	176.5	26	21.4 and 14
6:30	7.325	177	176.7	27	21.7 and 14
6:45	7.325	177	176.7	22	21.9 and 13
7:00	11.072	177	176.7	13	11.6
7:15	11.072	177	176.7	13	11.6
7:30	11.072	177	176.7	13	11.6
7:45	11.072	177	176.7	13	11.6
8:00	11.072	177	176.7	13	11.6
8:15	11.072	177	176.7	13	11.6
11:00	11.072	178	176.8	11	11.6
11:15	11.072	177	176.8	11	11.6
11:30	11.072	177	176.8	12	11.6
11:45	11.072	177	176.8	12	11.6
12:00	11.072	177	176.8	12	11.6

Table 8. Values of measured and calculated arrival angles of ray trajectories for those moments of the day on 06/22/2020 when the calculated MUF for the ordinary wave was less than the

signal frequency in the experiment

Time UT	Signal frequency in the experiment, MHz	Calculated MUF, MHz	Measured azimuth, deg	Azimuth calculated for the calculated MUF, deg	Measured elevation angle, deg	Elevation angle calculated for the calculated MUF, deg
8:30	12.114	11536	176	176.7	13	11.6
8:45	12.114	11.533	177	176.8	13	11.6
9:00	12.114	11.531	177	176.8	13	11.6
9:15	12.114	11.529	178	176.8	13	11.6
9:30	12.114	11.528	176	176.7	13	11.6
9:45	12.114	11.527	178	176.8	13	11.6
10:00	12.114	11.527	177	176.8	13	11.6
10:15	12.114	11.528	177	176.8	13	11.6
10:30	12.114	11.530	177	176.8	13	11.6
10:45	12.114	11.532	177	176.8	13	11.6

Figure captions

Fig. 1. Active phased antenna arrays in the form of a ring of masts, on which either transmitting or receiving antennas are located. The receiving and transmitting antenna arrays are designed as ring equidistant antenna systems.

Fig. 2. Projections onto the vertical plane passing through the receiver and transmitter of the ray trajectory for the ordinary wave at a frequency of 7.271 MHz for the time moment 6:15 UT 21.06.2019 (top) and the ray trajectory for the ordinary wave at a frequency of 11.072 MHz for the time moment 8:15 UT 21.06.2019 (bottom). The background shows the distributions on the specified plane of the plasma frequency divided by 2 π in MHz, calculated using the GDMI model for the specified time moments.

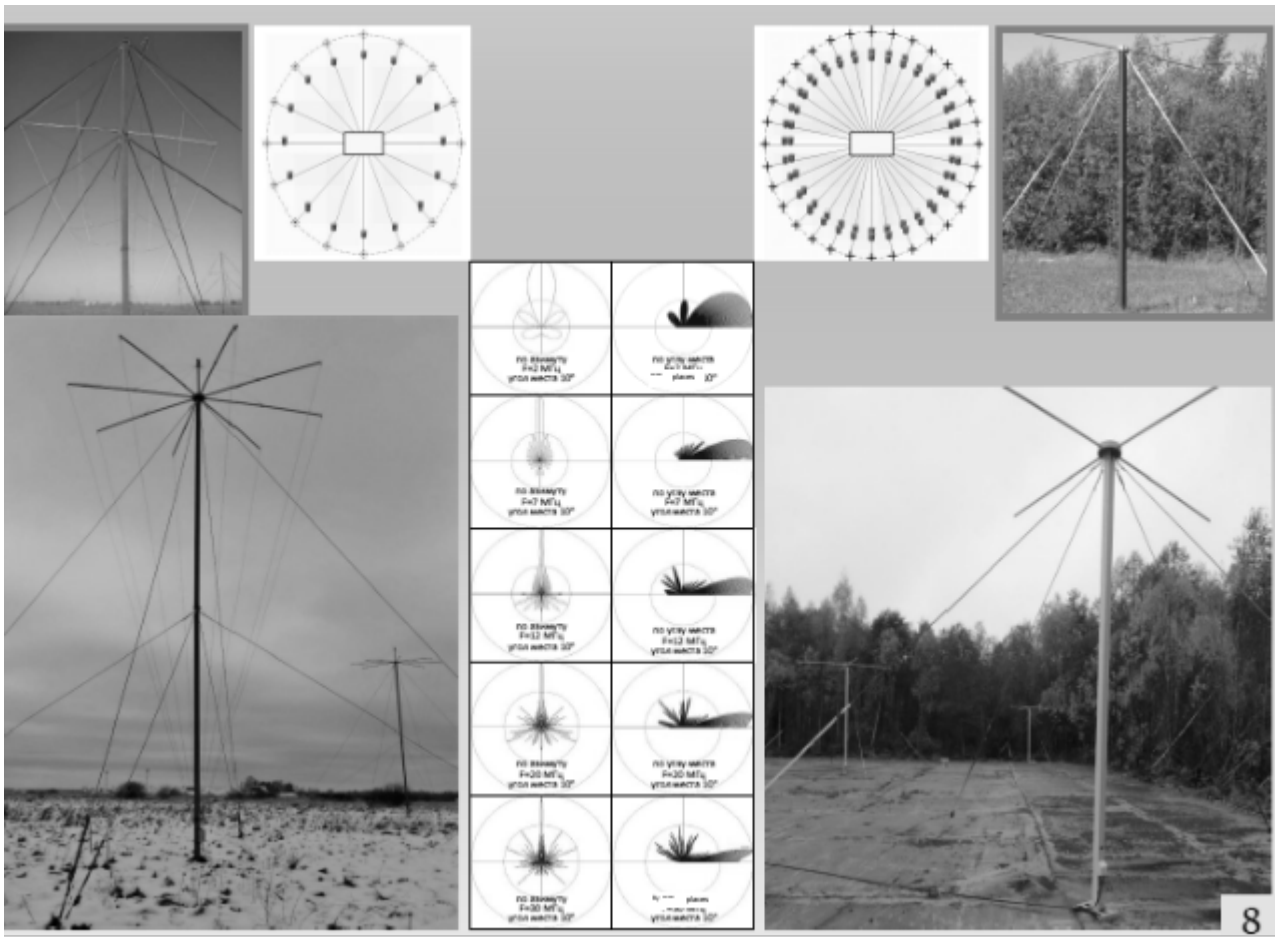

Fig. 1.

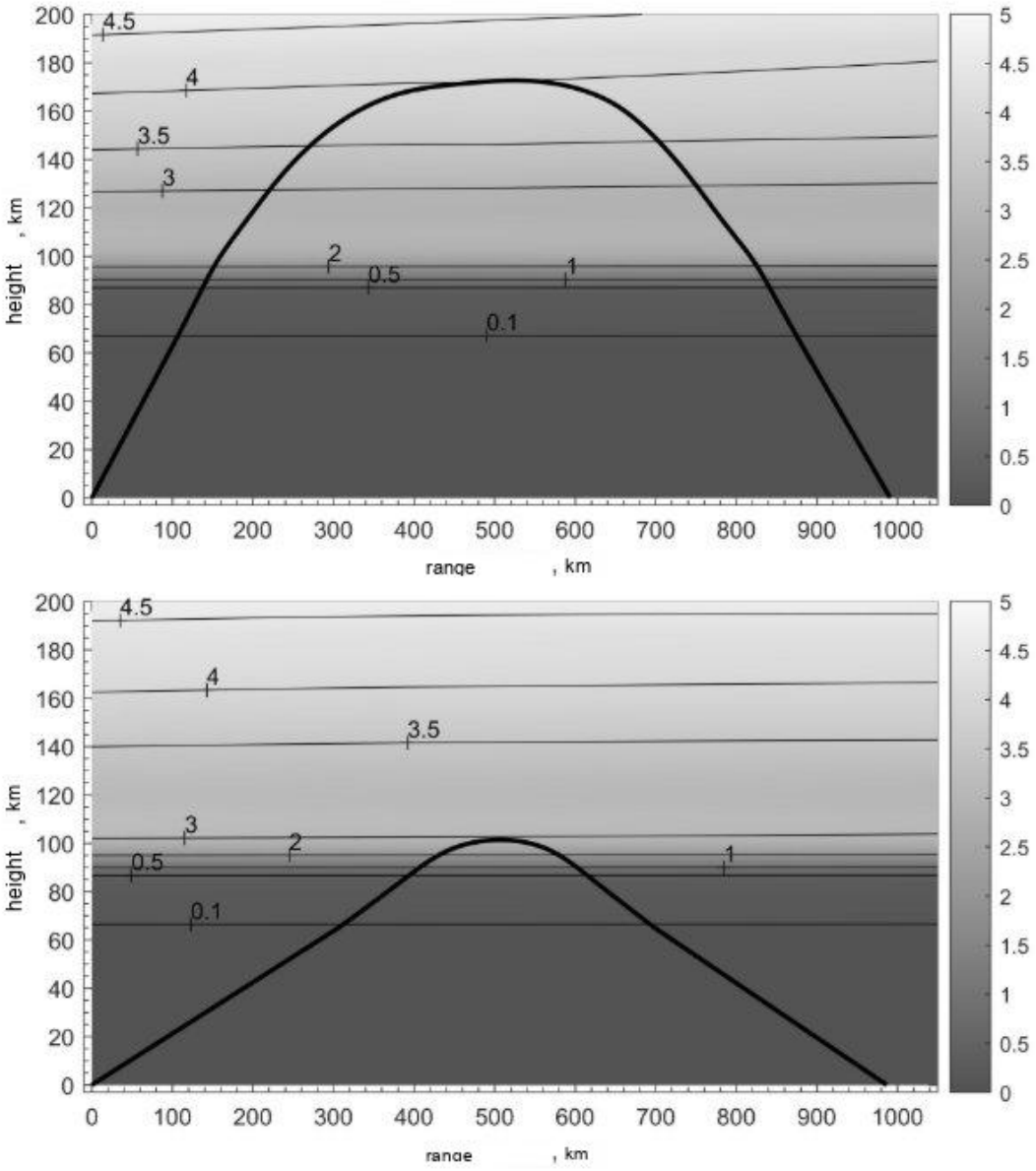

Fig. 2.